CO_2 reforming of methane over Ni-Ru supported catalysts: on the nature of active sites by *operando* DRIFTS study

A. Álvarez M., L.F. Bobadilla*, V. Garcilaso, M.A. Centeno and J.A. Odriozola

[1] *Instituto de Ciencia de Materiales de Sevilla, Centro mixto Universidad de Sevilla-CSIC, 49 Av. Américo Vespucio, 41092 Sevilla, Spain*

* Corresponding author: bobadilla@icmse.csic.es (Luis F. Bobadilla)

Abstract: The present paper addresses the nature of the active sites of a bimetallic Ni-Ru supported catalyst on the dry reforming of methane (DRM). The structural characterization by XRD and Raman spectroscopy, along with the reducibility study (TPR-H_2) of the samples, evidenced the existence of a strong Ni–Ru interaction in the bimetallic system. We have assumed that Ru atoms block the most reactive Ni sites (step-edge sites) leaving less reactive centers for methane activation (terraces). In this way, *operando* DRIFTS measurements revealed that Ru decreases the catalytic activity but favors the carbon gasification and prevents the CO dissociation.

Keywords: Dry reforming of methane; Ni-Ru bimetallic; operando DRIFTS

1. Introduction

CO_2 conversion into value-added chemicals such as syngas, methanol or dimethylether (DME) is considered as the ideal route for dealing with global warming, energy crisis, and energy storage [1-3]. Therefore, any efficient reactions using CO_2 as a reagent have positive effects towards carbon management.

Among the different possible reactions, the transformation of CO_2 with CH_4 (Eq.1) stands out due to the abundance of these reactants and the possibility of their transformation towards H_2 and/or synthesis gas (syngas).

$$CH_4 + CO_2 \rightarrow 2CO + 2H_2 \qquad \text{(Eq. 1)}$$

This reaction, known as CO_2 or dry reforming of methane (DRM), is highly endothermic and thus require high operating temperatures to reach high conversions of the reactants. However, these high temperatures result in catalyst deactivation by coke deposition, mainly due to the deep cracking of methane [4, 5]. Hence, it is a major challenge to develop highly thermal resistant catalysts which can inhibit carbon deposition effectively.

Noble metal-based and Ni-based catalysts are the most widely used for DRM. From the industrial standpoint, nickel is more attractive since it is more accessible and less expensive, so high loadings are feasible in order to achieve a high catalytic performance. Nevertheless, Ni-based catalysts get easily deactivated by sintering, coke deposition and Ni oxidation. Several approaches have been demonstrated to be feasible in order to increase its stability. For instance, the modification of the support acid-base properties is a plausible alternative since the formation of coke in oxide supports is the result of the acid-catalyzed cracking and polymerization reactions between the coke precursors [6, 7]. Wang at al. [8] reported that the addition of basic elements as Na or Mg reduce the carbon formation in a 13.4%. Horiuchi et al. [9] reported that the addition of Na, K, and Mg decreases the carbon formation owed to the lower catalyst capacity to adsorb dissociatively CH_4. Bobadilla et al.[10] established an optimum quantity of MgO in 10

wt.% that allowed the modification of the support acidity and improved the Ni dispersion. In addition, other strategies have been addressed regarding the active phase modification. Trimm [11, 12] proposed the formation of Ni-M (M= Sn, Ge…) alloys where, hypothetically, the 3d electrons of Ni are interacting with the 2p electrons of the alloying metal (M), avoiding in this way the formation nickel carbide, which they propose, is the main precursor in coke formation. The addition of noble metals is another strategy to improve the resistance to deactivation. Pt [13, 14], Rh [15, 16] or Ru [17, 18], have been successful approached. Additionally, besides improving the catalyst resistance towards coke deposition, the addition of noble metals enhances the catalytic activity. Nevertheless, when Ni catalysts are modified with small amounts of another metal, a lot of attention have been paid to the preparation method. In this sense, we have previously demonstrated how the metal order addition have a huge influence in a bimetallic Ni-Ru catalyst when performing the combined steam-dry reforming of methane [19].

In the last decades, numerous efforts have been focused in the elucidation of the reaction mechanism and the elementary steps of dry reforming of methane. However, the nature of the adsorbed species, as well as the key reaction intermediates is still controversial. To gain a more comprehensive vision of the role of the involved species during the DRM it is necessary to make use of spectroscopic techniques under reaction conditions, i.e., *in situ* and *operando* characterization methods. The purpose of the *operando* spectroscopy is to determine the active sites of the catalyst and the spectator species present during the reaction under working conditions. Diffuse reflectance infrared Fourier transform spectroscopy (DRIFTS) has been widely employed as a useful tool to investigate the adsorbed species during the reaction and to elucidate the mechanism by correlating the structure of the catalyst and intermediates with the catalytic activity/selectivity. The present paper deals with a comprehensive study to understand the nature of the active sites of a Ni-Ru/MgO/Al_2O_3 catalyst in the DRM reaction and

clarify why the Ni-Ru combination increases the resistance towards carbon deposition under reaction conditions.

2. Experimental

2.1. Catalysts preparation

The MgO/Al_2O_3 support was prepared from a commercial γ-Alumina (Spheralite SCS505) sieved between 100-200 μm by impregnating an alcoholic solution of $Mg(NO_3)_2{\cdot}6H_2O$ (Aldrich) in order to obtain a 10 wt.% of MgO. In previous works [10, 20] we established that this quantity of MgO is the most adequate in order to assure an optimal acidity/basicity of the support and guarantee a good Ni dispersion. After impregnation, the solid was dried overnight at 100 ºC and then calcined for 12h at 850 ºC. This modified Al_2O_3 support was named "MgAl". Ni-Ru bimetallic catalyst was prepared by incipient wetness impregnation of both alcoholic solutions of $Ni(NO_3)_2.6H_2O$ (Panreac) and $Ru(NO)(NO_3)_3$ (Aldrich) mixed and impregnated simultaneously onto the support. After drying in air at 120 ºC overnight, the catalysts were calcined in air at 500 ºC for 5 h. Ni and Ru monometallic catalysts were prepared by simple impregnation following an analogous procedure. The nickel and ruthenium contents were fixed at 15 wt.% and 0.5 wt.%, respectively. Bimetallic catalyst was denoted as NiRu/MgAl while the Ni and Ru monometallic catalysts were labelled as Ni/MgAl and Ru/MgAl, respectively.

2.2. Characterization techniques

Metal content of the catalysts was determined by X-ray fluorescence spectrometry (XRF) in a PAnalytical AXIOS PW440 sequential spectrophotometer with a rhodium tube as source of radiation. Textural properties of calcined catalysts were investigated by nitrogen adsorption experiments at liquid nitrogen temperature. The measurements were performed using a Micromeritics ASAP 2010 equipment. Prior to the analysis, the samples were degassed for 2 h at 250 ºC in vacuum to remove surface impurities. The structure of the catalysts was analyzed by X-ray diffraction (XRD) on an X'Pert Pro

PANalytical Diffractometer. Diffraction patterns were recorded with Cu Kα radiation (40 mA, 45 kV) over a 2θ range of 10–80º and a position-sensitive detector using a step size of 0.05º and a step time of 1 s. Raman spectra were collected on a dispersive Horiba Jobin Yvon LabRam HR800 microscope with a 20 mW He–Ne green laser (532.14 nm) operating at 5 mW and with a 600 g mm^{-1} grating. A 50X objective (Olympus) was used for both focusing the excitation beam on the sample and collecting the scattered light with a confocal pinhole of 1000 μm. Temperature programmed reduction (TPR) measurements were performed by means of a Micromeritics AutoChem II 2920 equipment with a TCD detector. The analysis was carried out using 100 mg of fresh catalyst under 25 mL min^{-1} of a 10% H_2/Ar mixture. The temperature was increased from room temperature to 950 ºC with a rate of 10º min^{-1}. The H_2 consumption was continuously monitored on a thermal conductivity detector (TCD). CuO powder was used as standard for calibrating the H_2 consumption. The degree of reducibility was estimated assuming that only Ni^{2+} and/or Ru^{2+} were present like reducible species in the samples before the reduction pretreatment.

2.3. Activity measurements

The dry reforming of methane was carried out in a commercial computerized Microactivity Reference Catalytic Reactor from PID Eng&Tech, employing a stainless steel reactor with 9 mm internal diameter. A catalytic bed of 0.32 cm^3 composed by 50 mg of catalyst diluted in SiC (both sieved in 100-200 μm) was placed in the center of the reactor. Prior to the reaction, the catalyst was reduced in 50% H_2/N_2 at 750 °C for 3 h (100 mL min^{-1}). After the pretreatment, a feed mixture of $CO_2/CH_4/N_2$ (2:2:1) with a CH_4/CO_2 = 1 molar ratio at a total flow rate of 115 mL min^{-1} was introduced into the reactor. The total space velocity was equal to 150 L h^{-1} g^{-1}. The reforming tests were performed at 650, 600 and 550 °C in decreasing order maintaining each temperature for 2 h to achieve steady-state conditions. The effluent gases were analyzed on line by using

a micro Gas Chromatograph (Varian 4900 model) equipped with two columns: Poraplot Q and Molecular Sieve 5A.

2.4. *Operando* DRIFTS study

Operando DRIFTS measurements were performed in a high-temperature environmental reaction cell supported in a Praying Mantis (Harrick) optical system with ZnSe windows. The spectra were recorded on a Thermo Nicolet Nexus FTIR spectrometer equipped with a liquid N_2 cooled MCT detector at 4 cm^{-1} of resolution and an average of 64 scans. About 50 mg of catalyst was loaded in the cell for each experiment. Prior to the measurements, the catalyst was activated in situ at 750 ºC in 50% H_2/Ar with a total flow of 50 mL min^{-1}. The reaction was performed by feeding a mixture of 10% of CH_4 and 10% of CO_2 in argon balance for a total flow rate of 50 mL min^{-1} into the DRIFTS cell. The temperature was increased from 550 ºC to 700 ºC with intervals of 50 ºC and each temperature was maintained for 30 min to achieve steady-state conditions. For the experiment of CO_2 adsorption, a total flow rate of 50 mL min^{-1} of 10% CO_2 in Ar was introduced into the IR cell for 30 min under isothermal conditions at 550 ºC. Typically, 64 scans were collected at 4 cm^{-1} resolution in the range of 400 – 4000 cm^{-1}. In both experiments, the concentration of CO_2 was measured by time-resolved analysis by using a VAISALA CO_2 analyzer and all DRIFT spectra of the adsorbed species on the catalyst surface were obtained by subtracting the spectrum of the catalyst after reduction pretreatment.

3. Results and discussion

3.1 Structural analysis and textural properties

XRF results (Table 1) show that the metal content of Ni and Ru are close to the desired values (15 wt.% of Ni and 0.5 wt.% of Ru) in all catalysts prepared. Regarding the textural properties, all solids are mesoporous (adsorption and desorption isotherms are Type IV, not shown), and the textural properties are mainly governed by the support. However,

there is a slight decrease in the S_{BET} area, pore volume and pore size when Ni and/ or Ru are added, indicating a slight blocking of the porosity by the metal addition (Table 1).

******** INSERT TABLE 1 HERE ********

Figure 1 presents the XRD patterns of the calcined catalysts as well as that of support. As observed, the principal and more intense peaks correspond to the $MgAl_2O_4$ spinel (JCPDS 00-021-1152). The coexistence of $MgAl_2O_4$ with a minor amount of $NiAl_2O_4$ spinel should not be discarded, although at the temperature at which the catalysts have been calcined (500 ºC) thermodynamically is favoured the preferential formation of $MgAl_2O_4$ [20]. The absence of peaks associated to MgO phase implies that the impregnation of 10 wt.% of MgO and subsequent calcination, results into the total insertion of Mg^{2+} into the tetrahedral sites of the initial alumina. The formation of $MgAl_2O_4$ has been widely studied as a beneficial aspect in reforming catalysts since it enhances Ni dispersion, decreases the alumina acidity and increases the CO_2 adsorption capacity [21-23]. Regarding the metal phases, Ni is evidenced as NiO (JCPDS 00-047-1049) and Ru as RuO_2 (JCPDS 01-070-2662). Scherrer calculation of the NiO crystallite size indicates no great differences between the samples, finding an average size of 5-6 nm. Regarding Ru, Scherrer crystallite size calculations denote a size around 30 nm for the Ru/MgAl sample whereas for the NiRu/MgAl no signs of RuO_2 are evidenced. This could be owed to a high dispersion of RuO_2 or even to a possible NiO-RuO_2 mixed-oxide.

******** INSERT FIG. 1 HERE ********

In order to clarify the RuO_2-NiO interaction, a Raman analysis of the calcined samples was performed (Figure 2). The bands at 410 and 711 cm^{-1}, characteristic of the E_g and A_{1g} vibration modes of $MgAl_2O_4$, validate the formation of the $MgAl_2O_4$ spinel [24]. Regarding the monometallic samples, the Ru/MgAl present the characteristic bands of RuO_2, at 510, 625, and 700 cm^{-1}, corresponding to the E_g, A_{1g} and B_{2g} vibration modes, respectively [25, 26]. Meanwhile, the Ni/MgAl sample presents a broad band around 550

cm^{-1} that can be related to two overlapping bands attributed to first order transverse optical (TO) and longitudinal (LO) phonon modes of NiO [27-29]. As it can be noted, the bimetallic sample present a different behavior. Noteworthy that the wide band around 550 cm^{-1} comprises the LO phonon mode of NiO and the E_g mode of RuO_2. Nevertheless, the A_{1g} mode of RuO_2 in this sample is very weak. It has been described that the variation of the lattice parameters of RuO_2 may cause stress and limit the A_{1g} mode, weakening this band. The structural modification owed to the variation of particle size, or even de insertion of Ni^{2+} into the RuO_2 lattice could cause this variation in the Raman spectra. This behavior has been previously reported by our group and denotes a high RuO_2-NiO interaction [19].

******** INSERT FIG. 2 HERE ********

The reducibility of Ni^{2+} and RuO_2 species supported on MgAl was investigated by H_2-TPR measurements. Their profiles are reported in Figure 3. Regarding the monometallic samples, the Ru/MgAl present an unique peak at 200ºC attributed to the reduction of Ru^{+4} to metallic Ru [30, 31] while the Ni/MgAl catalyst present a broad peak around 600 ºC and a smaller one at very high temperature (~850 ºC). The broad peak can be ascribed to the reduction of Ni^{2+} to Ni^0 in isolated NiO [32] whereas the small shoulder at higher temperature can be attributed to the reduction of Ni in strong interaction with the support, forming probably the $NiAl_2O_4$ spinel as we suggested above. Considering that the amount of MgO added to the initial alumina support was of 10 wt.% and that the total available tetrahedral sites available in the γ-Al_2O_3 accounts for 28 wt.%, there are still “free” tetrahedral sites which Ni can occupy and form the Ni-Al spinel ($NiAl_2O_4$). In good agreement, the Ni reduction in the $NiAl_2O_4$ spinel has been widely studied and has been reported to present Ni reduction peaks around 800 ºC [33-35]. Likewise, it is worth to notice the shape of the reduction peaks between 400 and 650 ºC of the bimetallic sample. When Ru is present, the maximum reduction temperature of Ni shifts toward lower values, indicating a positive effect of Ru in the reduction of Ni, probably owed to

spillover phenomena. Enger et al. [36] describe that noble metals are able to promote the reduction of Ni owed to the electronic effects and spillover phenomenon indicating that an intimate contact between both metals should exist in order to observe these effect. This statement is in agreement with the results observed in the bimetallic catalyst where a major percentage of Ni is reduced at lower temperature compared to the Ni/MgAl monometallic sample. Equally, when comparing the experimental H_2 consumed with the theoretical values, a higher percentage of reducibility is observed for this sample (Table 1). The increase in the reducibility percentage as well as the shift toward lower temperature in the TPR profile, besides the strong evidence of higher Ni-Ru interaction observed by Raman spectroscopy, suggest that the presence of Ru could promote the formation of a Ni-Ru alloy and increase the Ni dispersion, although there is no full evidences of possible Ni-Ru alloy formation.

******** INSERT FIG. 3 HERE ********

3.2. Comparative catalytic performance for the DRM reaction

Catalytic activity for Ni, Ru and Ni-Ru supported on MgAl was evaluated for the DRM reaction in the temperature range of 650-550 ºC. Fig.4 shows the CO_2-CH_4 conversions and the H_2/CO molar ratio obtained as a function of time at each temperature for the three catalysts studied. We note that Ni/MgAl catalyst exhibits the most optimal catalytic performance whereas monometallic Ru sample is the less active. H_2/CO molar ratios lower than one were observed during methane dry reforming in the three cases. This is attributed to the reverse water-gas shift (RWGS) reaction (Eq.2), in which part of the hydrogen produced is consumed in the reaction with CO_2.

$$CO_2\ (g) + H_2\ (g) \leftrightarrow CO\ (g) + H_2O\ (g) \qquad \text{(Eq. 2)}$$

We would like to emphasize here the rate for RWGS is higher than methane decomposition, and thus the RWGS reaction achieve rapidly the equilibrium [37].

******** INSERT FIG. 4 HERE ********

This order for DRM reactivity is opposite to the results previously reported for the combined steam-dry reforming in which the bimetallic Ni-Ru catalyst presented the highest catalytic activity [19]. It is generally accepted that the reaction of steam reforming of methane (SRM) proceeds via dehydrogenation of methane to form surface carbon which is oxidized by adsorbed oxygen generated from water dissociation [38] The thermodynamics of SRM favors the formation of nickel oxide and the role of Ru on the Ni-Ru alloy is to activate the hydrogen produced by the dehydrogenation of CH_4 through a spillover effect enhancing the reduction of Ni^{2+} species originally present or formed over the catalysts [39]. Moreover, the presence of water enhances the gasification of carbonaceous deposits and it is well known the presence of Ru favors this reaction [40]. By contrast, the DRM reaction occurs via decomposition of methane to generate surface carbon and hydrogen species followed by the subsequent reaction of surface carbon with CO_2 to produce CO (Boudouard reaction) [41]. In this case, the thermodynamics of DRM favor the formation of nickel carbide or carbon, and the role of ruthenium has not been completely clarified. Our results show that the addition of ruthenium decreases the DRM intrinsic activity of monometallic Ni catalyst, and it could be caused by local changes in the electronic structure. Typically, the nickel surfaces present two types of active sites: terraces and edge-step sites. From a theoretical point of view, the reactivity of catalytic surfaces is often dominated by very reactive low-coordinated atoms such as step-edge sites [42]. Different studies on model surfaces have concluded that activation of methane depends sensitively on surface structure; specifically, surface steps and kinks are much more active than atoms on terraces [43]. Although additional characterization such as XPS would be necessary to be confirmed, we believe that the subsequent addition of Ru decreases the activity because of atoms of Ru are located on the step-edge sites of Ni particles and the blockage of these reactive step-edge sites on Ni surfaces shifts the active centers for methane activation from step sites to less reactive terrace sites as have been previously reported for other analogous cases like the combination Ni-Ag [44] or Ni-Au [45]. We have assumed the atoms of Ru are located on

the step-edge sites considering the limited solubility between nickel and ruthenium. Consequently, although the concentration of Ru is very low it can be sufficient to block the Ni active sites.

3.3. *Operando* DRIFTS study of dry reforming reaction

Operando DRIFTS was used to investigate the nature of the active sites and the adsorbed species on the catalyst surface during the DRM reaction in the temperature range of 550 – 700 ºC. Fig. 5 shows the spectra recorded under steady-state conditions over the mono- and bimetallic Ni-Ru catalysts after stabilization of the reaction mixture at 550, 600, 650 and 700 ºC. IR spectra of the catalysts taken under reaction conditions present bands in two regions, one set appearing between 3600 and 2700 cm^{-1} and another set appearing between 2600 and 1200 cm^{-1}. The bands in the first of these regions are associated with hydroxyls groups and hydrocarbons where slight perturbations were observed due to the possible formation of water and methane in gas phase, respectively. The bands appearing in the second region are due to CO_2 and CO gas, carbonyl and carbonate species. The effects of the reaction temperature on the spectra of the adsorbed species present on the surface of the metal and/or support and the bands associated with the gas phase were evaluated with detail to identify the stability and reactivity of these species in the DRM reaction.

******** INSERT FIG. 5 HERE ********

The bands appearing at 1637, 1590 and 1377 cm^{-1} are characteristic of carbonates with different degree of coordination on the $MgAl_2O_4$ support [46]. These species are formed by direct adsorption of CO_2 on the support towards the interaction with the hydroxyl groups and they are present in the three samples in all the range of temperature investigated. The intense bands observed in the 2100-1900 cm^{-1} range correspond to metallic carbonyl species. The band observed at 2020-2030 cm^{-1} is characteristic of CO coordinated linearly on metal sites (Ni^0-CO), whereas the vibrational mode at 1910 cm^{-1}

indicate the formation of bridging carbonyls ($(Ni^0)_x$-CO) [47]. However, the absence of bands associated with Ru carbonyls in the monometallic catalyst is evidenced. Likewise, the shift in the frequencies of Ni carbonyls in the Ni-Ru/MgAl catalyst, associated to the Ni-Ru interaction is not observed. This fact is due to the high Ni/Ru ratio (Ni~15%; Ru~0,5%) in the bimetallic catalyst where the effects are masked. On the other hand, the monometallic Ru catalyst present a band at 1980 cm^{-1} that is typical of bridging-bonded CO on Ru zerovalent sites with a slightly different energy and could be attributed to the decrease in the CO surface coverage, which allows the transformation of linearly to bridged bonded sites at higher temperatures [48]. This suggest that CO_2 is dissociated on Ru sites forming CO linearly bonded on Ru that rapidly are desorbed to gas phase CO and only remain on the catalyst surface the Ru bridged-adsorbed CO species. As can be observed, by increasing the reaction temperature the band areas of gas phase CO_2 and CH_4 are decreased whereas the CO produced is increased. Figure 6 shows the CO_2 conversion measured during the *operando* DRIFTS experiments for the three catalysts. We observe that the values found of CO_2 conversion in the DRIFTS cell are consistent with the values obtained in the chemical reactor indicating that the *operando* methodology used involves *true* catalytic kinetic conditions.

******** INSERT FIG. 6 HERE ********

Ni is more active than Ru for the CO_2 dissociation. Nevertheless, CO can be desorbed from Ru sites before further decomposition whereas may be decomposed into carbon on Ni before desorption [49]. This implies that the Ni-catalyst can be rapidly deactivated by coke deposition. Although the combination Ni-Ru is less active for the DRM activation, we believe that the presence of ruthenium in intimal contact with the active nickel helps to mitigate the carbon formed avoiding the formation of nickel carbide. The role of Ru is to decrease the diffusion rate of carbon into the metallic nickel particle avoiding the growth of the carbon nanotubes [7].

In order to confirm this assumption we have represented the evolution of the band associated to CO linearly adsorbed and the area of the band associated to gas phase CO against the CO_2 rate consumption for both Ni- and NiRu catalysts (Fig. 7a and 7b, respectively). It is evidenced that a linear correlation exists between the CO produced in gas phase and the CO_2 dissociated to CO linear species in both catalysts. Aditionally, a clear deviation of the slope in the CO production and the linear carbonyls representation is evidenced for the monometallic sample, suggesting that the reaction proceeds with another reaction path at greater temperatures.

******** INSERT FIG. 7 HERE ********

Between the expected reactions in the catalyst surface, the Bouduard reaction (Eq. 3) and the RWGS reaction (Eq. 2) are the main responsible for the increase of CO_2 rate and CO production.

$$CO_2\ (g) + C(s) \leftrightarrow 2CO\ (g) \qquad \text{(Eq. 3)}$$

Between 500 ºC and 600 ºC, the RWGS reaction begins to be thermodynamically favorable and the CO production is mainly associated to this reaction. However, in this range of temperature the carbon deposition is increased due to the reverse Boudouard reaction, which is highly exothermic and present a greater preference towards carbon deposition at low temperature [50, 51]. From 600 ºC to 700 ºC, the carbon deposition decreases due to an increase in the thermodynamic favorability of the Boudouard reaction. At higher temperatures, the methane decomposition is very favored but the carbon formed reacts with the CO_2 producing CO. This reaction is thermodynamically very favorable around 700 ºC and the CO_2 consumption and the CO production depend essentially on this reaction, but the rate reduces when CO_2 is the limiting reactant [52]. This explains the slight deviation of the slopes observed for CO production and linearly adsorbed CO on the monometallic Ni catalyst. It can be inferred from these observations that the results obtained are consistent with the thermodynamic and kinetic predictions.

Noteworthy that this deviation is not observed in the Ni-Ru bimetallic catalyst. To understand the effect of Ru it must be considered the others reaction involved in the process such as the carbon gasification (Eq. 4 and Eq. 5):

$$C\ (s) + H_2O\ (g) \leftrightarrow CO\ (g) + H_2\ (g) \qquad \text{(Eq. 4)}$$

$$C\ (s) + 2H_2O\ (g) \leftrightarrow CO_2\ (g) + 2H_2\ (g) \qquad \text{(Eq. 5)}$$

The water formed in the RWGS reaction can react with the carbon adsorbed species producing CO_x and hydrogen. This reaction requires the activation of the water molecules and the presence of Ru promotes this step. Since the electronic density of ruthenium is higher than of nickel, the Ni-Ru interaction results in the modification of the oxidation state of Ni and Ru, respectively. The nickel on the coordination sphere of the Ru atoms acquires a higher electronic density, thus decreasing the number of coordination and consequently the surface energy. This suggests that Ru addition decreases the stability of the Ni neighboring sites and thus the stability of the adsorbed carbon species. On the other hand, the Ni-Ru interaction decreases the electronic density on Ru sites and therefore increases its oxophilicity favoring the water dissociation. A similar case have been already reported by ourselves for a bimetallic Ni-Au catalyst [53]. Therefore, is precise to suggest that the presence of Ru favors the carbon gasification implied in the DRM reaction.

3.4. DRIFTS study of CO_2 adsorption

In order to explore details of the CO_2 activation, we performed an experiment of CO_2 adsorption at 550 ºC on both monometallic Ni and the bimetallic Ni-Ru catalysts. Figure 8 shows the IR spectra of the surface species formed in both catalysts during CO_2 exposure. We can note that the adsorption of CO_2 at 550 ºC leads to the appearance of several bands. Carbonates on the support are evidenced in the 1800 – 1350 cm^{-1} range, carbonyl species on the metallic sites are shown on the 2000 – 1800 cm^{-1} range and gas phase CO_2 is evidenced at 2349 cm^{-1} (not shown). The presence of carbonyls evidences

that dissociative adsorption of CO_2 takes place on the Ni-Ru sites whereas the formation of carbonates likely occurs on the basic sites of the support. It should be noted that on both samples appears the band ascribed to CO linearly adsorbed on Ni sites and a new band at 1830 cm^{-1} that is characteristic of Ni multicentered carbonyl species of type $Ni_3(CO)$ and $Ni_4(CO)$ [54] while the band at 1910 cm^{-1} associated to bridging-carbonyls is apparently absent. We believe that CO_2 dissociation occurs on the edge-sites of the metal particle and the formed CO migrates to the terraces where it interacts with the atoms forming polynuclear carbonyl species. The absence of these species during the DRM reaction may be due to the presence of carbon adsorbed species that restrain the interaction of CO with a maximum of two atoms. Comparing both mono- and bimetallic samples, the position of the IR bands appeared are identical, although noteworthy that the proportion of carbonyls with respect to carbonates is significantly major in the bimetallic catalyst. This indicates that the presence of highly dispersed Ru interacting strongly with the nickel particles on the edge sites favors the CO_2 dissociation. In a recent theoretical study, it was calculated that on Ru (0001) surface the direct dissociation of CO_2 is thermodynamically favorable although with a significant activation barrier, suggesting the direct CO_2 dissociation does not readily takes place on close-packed Ru surfaces that are abundant in large Ru particles [55]. It should be mentioned that during the DRM reaction the CO_2 conversion was superior on monometallic Ni catalyst. This apparent inconsistency can be understood considering that monometallic Ni catalyst favors the methane decomposition reaction increasing the CO_2 conversion via Boudouard reaction, but in absence of methane CO_2 dissociation is more favored on bimetallic Ni-Ru catalyst.

******** INSERT FIG. 8 HERE ********

Figure 9 presents the temporal evolution of the IR band area of carbonyls and carbonates species and the concentration of gaseous CO_2 analyzed online. It can be appreciated in both samples that initially an important amount of gaseous CO_2 is trapped on the catalyst

surface forming carbonate species until the saturation is reached and another part of CO_2 is dissociated forming carbonyls species. As can be observed, the production of carbonyls is superior over the Ni-Ru catalyst showing that this catalyst favors the CO_2 dissociation. On the other hand, is noteworthy that the carbonyls curve reaches a maximum value and decreases till increases again slightly. This feature can be attributed to the dissociation of CO and subsequent reaction of carbon with CO_2 via Boudouard, and the effect is more pronounced on the monometallic catalyst. We can conclude that the presence of Ru favors the CO_2 dissociation but prevents the CO dissociation.

******** INSERT FIG. 9 HERE ********

4. Conclusions

The role of Ni and Ru in a bimetallic Ni-Ru catalyst on the dry reforming of methane reaction has been explored. The results of structural characterization and reducibility suggest that exist a strong interaction between both metals. Considering the low solubility between nickel and ruthenium, we have assumed the atoms of Ru are located on the more reactive step-edge sites and the active centers for methane activation are shift to the less reactive sites, the terraces. For this reason, the presence of Ru decreases notably the catalytic activity. However, *operando* DRIFTS measurements shown that the presence of Ru decreases the CO_2 conversion, favors the gasification of carbon adsorbed species and prevent the dissociation of CO.

Acknowledgments

Financial support for this work has been obtained from the Spanish Ministerio de Economía y Competitividad – MINECO (ENE2013-47880-C3-2-R and ENE2015-66975-C3-2-R) and from the Junta de Andalucía (TEP-8196) both co-financed by FEDER funds from the European Union. Luis F. Bobadilla thanks MINECO for the Juan de la Cierva Incorporación 2015 contract. Victoria Garcilaso thanks MINECO for the FPI fellowship (BES-2013-062806).

References

[1] I. Ganesh, Renew. Sustain. Energy Rev. 31 (2014) 221-257.

[2] J. Ma, N. Sun, X. Zhang, N. Zhao, F. Xiao, W. Wei, Y. Sun, Catal. Today 148 (2009) 221-231.

[3] F.D. Meylan, V. Moreau, S. Erkman, J. CO2 Util. 12 (2015) 101-108.

[4] M.C.J. Bradford, M.A. Vannice, Catal. Rev. 41 (1999) 1-42.

[5] S. Arora, R. Prasad, RSC Adv. 6 (2016) 108668-108688.

[6] C.H. Bartholomew, Catal. Rev. 24 (1982) 67-112.

[7] C.H. Bartholomew, Appl. Catal. A Gen. 212 (2001) 17-60.

[8] S. Wang, G.Q. Lu, J. Chem. Technol. Biotechnol. 75 (2000) 589-595.

[9] T. Horiuchi, K. Sakuma, T. Fukui, Y. Kubo, T. Osaki, T. Mori, Appl. Catal. A Gen. 144 (1996) 111-120.

[10] L.F. Bobadilla, A. Penkova, F. Romero-Sarria, M.A. Centeno, J.A. Odriozola, Int. J. Hydrogen Energy 39 (2014) 5704-5712.

[11] D.L. Trimm, Catal. Rev. 17 (1977) 155-189.

[12] D.L. Trimm, Catal. Today 37 (1997) 233-238.

[13] T.D. Gould, M.M. Montemore, A.M. Lubers, L.D. Ellis, A.W. Weimer, J.L. Falconer, J.W. Medlin, Appl. Catal. A Gen. 492 (2015) 107-116.

[14] Y. Mukainakano, K. Yoshida, S. Kado, K. Okumura, K. Kunimori, K. Tomishige, Chem. Eng. Sci. 63 (2008) 4891-4901.

[15] W.-J. Cai, L.-P. Qian, B. Yue, H.-Y. He, Chinese Chem. Lett. 25 (2014) 1411-1415.

[16] M. Ocsachoque, F. Pompeo, G. Gonzalez, Catal. Today 172 (2011) 226-231.

[17] C. Crisafulli, S. Scirè, S. Minicò, L. Solarino, Appl. Catal. A Gen. 225 (2002) 1-9.

[18] J.H. Jeong, J.W. Lee, D.J. Seo, Y. Seo, W.L. Yoon, D.K. Lee, D.H. Kim, Appl. Catal. A Gen. 302 (2006) 151-156.

[19] A. Álvarez M, M.Á. Centeno, J.A. Odriozola, Top. Catal. 59 (2016) 303-313.

[20] A. Penkova, L. Bobadilla, S. Ivanova, M.I. Domínguez, F. Romero-Sarria, A.C. Roger, M.A. Centeno, J.A. Odriozola, Appl. Catal. A Gen. 392 (2011) 184-191.

[21] J. Sehested, J. Catal. 217 (2003) 417-426.

[22] H. Eltejaei, H. Reza Bozorgzadeh, J. Towfighi, M. Reza Omidkhah, M. Rezaei, R. Zanganeh, A. Zamaniyan, A. Zarrin Ghalam, Int. J. Hydrogen Energy 37 (2012) 4107-4118.

[23] A.M. Gadalla, B. Bower, Chem. Eng. Sci. 43 (1988) 3049-3062.

[24] M.P. O'Horo, A.L. Frisillo, W.B. White, J Phys. Chem. Solids 34 (1973) 23-28.

[25] L.-j. Meng, V. Teixeira, M.P. dos Santos, Thin Solid Films 442 (2003) 93-97.

[26] A. Korotcov, H.P. Hsu, Y.S. Huang, P.C. Liao, D.S. Tsai, K.K. Tiong, J. Alloy Comp. 442 (2007) 310-312.

[27] S.K. Yadav, P. Jeevanandam, J. Alloys Comp. 610 (2014) 567-574.

[28] W. Wang, Y. Liu, C. Xu, C. Zheng, G. Wang, Chem. Phys. Lett. 362 (2002) 119-122.

[29] G. Zhu, C. Xi, H. Xu, D. Zheng, Y. Liu, X. Xu, X. Shen, RSC Adv. 2 (2012) 4236-4241.

[30] P.G.J. Koopman, A.P.G. Kieboom, H. van Bekkum, J. Catal. 69 (1981) 172-179.

[31] I. Balint, A. Miyazaki, K.-i. Aika, React. Kinet. Catal. Lett. 80 (2003) 81-87.

[32] Y. Qiu, J. Chen, J. Zhang, Front. Chem. Eng. China 1 (2007) 167-171.

[33] M.L. Dieuzeide, V. Iannibelli, M. Jobbagy, N. Amadeo, Int. J. Hydrogen Energy 37 (2012) 14926-14930.

[34] E. Salehi, F.S. Azad, T. Harding, J. Abedi, Fuel Process. Technol. 92 (2011) 2203-2210.

[35] F.F. de Sousa, H.S.A. de Sousa, A.C. Oliveira, M.C.C. Junior, A.P. Ayala, E.B. Barros, B.C. Viana, J.M. Filho, A.C. Oliveira, Int. J. Hydrogen Energy 37 (2012) 3201-3212.

[36] B.C. Enger, R. Lødeng, A. Holmen, Catal. Lett. 134 (2010) 13-23.

[37] J. Wei, E. Iglesia, J. Catal. 224 (2004) 370-383.

[38] A. Al-Ubaid, E.E. Wolf, Appl. Catal. 40 (1988) 73-85.

[39] I. Luisetto, C. Sarno, D. De Felicis, F. Basoli, C. Battocchio, S. Tuti, S. Licoccia, E. Di Bartolomeo, Fuel Process. Technol. 158 (2017) 130-140.

[40] L.M.M. T, M. Araque, M.A. Centeno, A.C. Roger, Catal. Today 242 (2015) 80-90.

[41] A.R. González, Y.J.O. Asencios, E.M. Assaf, J.M. Assaf, Appl. Surf. Sci. 280 (2013) 876-887.

[42] R.T. Vang, K. Honkala, S. Dahl, E.K. Vestergaard, J. Schnadt, E. Laegsgaard, B.S. Clausen, J.K. Norskov, F. Besenbacher, Nat. Mater. 4 (2005) 160-162.

[43] J. Wei, E. Iglesia, J. Phys. Chem. B 108 (2004) 4094-4103.

[44] M. Yu, Y.-A. Zhu, Y. Lu, G. Tong, K. Zhu, X. Zhou, Appl. Catal. B Environ. 165 (2015) 43-56.

[45] F. Besenbacher, I. Chorkendorff, B.S. Clausen, B. Hammer, A.M. Molenbroek, J.K. Nørskov, I. Stensgaard, Science 279 (1998) 1913-1915.

[46] C. Morterra, G. Ghiotti, F. Boccuzi, S. Coluccia, J. Catal. 51 (1978) 299-313.

[47] G. Poncelet, M.A. Centeno, R. Molina, Appl. Catal. A Gen. 288 (2005) 232-242.

[48] S.Y. Chin, C.T. Williams, M.D. Amiridis, J. Phys. Chem. B 110 (2006) 871-882.

[49] M.J. Hei, H.B. Chen, J. Yi, Y.J. Lin, Y.Z. Lin, G. Wei, D.W. Liao, Surf. Sci. 417 (1998) 82-96.

[50] B. Abdullah, N.A. Abd Ghani, D.-V.N. Vo, J. Clean. Prod. 162 (2017) 170-185.

[51] J.Y. Lim, J. McGregor, A.J. Sederman, J.S. Dennis, Chem. Eng. Sci. 152 (2016) 754-766.

[52] M.K. Nikoo, N.A.S. Amin, Fuel Process. Technol. 92 (2011) 678-691.

[53] S. Palma, L.F. Bobadilla, A. Corrales, S. Ivanova, F. Romero-Sarria, M.A. Centeno, J.A. Odriozola, Appl. Catal. B Environ. 144 (2014) 846-854.

[54] M. Primet, J.A. Dalmon, G.A. Martin, J. Catal. 46 (1977) 25-36.

[55] S.-T. Zhang, H. Yan, M. Wei, D.G. Evans, X. Duan, RSC Adv. 4 (2014) 30241-30249.

TABLES AND FIGURES

Table 1. Metal loading, textural properties and reducibility of the catalysts prepared

Sample	Ni wt.%	Ru wt.%	S_{BET} $m^2\ g^{-1}$	Pore volume $cm^3\ g^{-1}$	Pore size nm	Reducibility %
MgAl support	0	-	123	0.37	9.5	-
Ni/MgAl	17.2	-	106	0.30	8.7	62
Ru/MgAl	-	0.41	118	0.35	9.3	82
Ni-Ru/MgAl	15.2	0.35	102	0.28	8.6	80

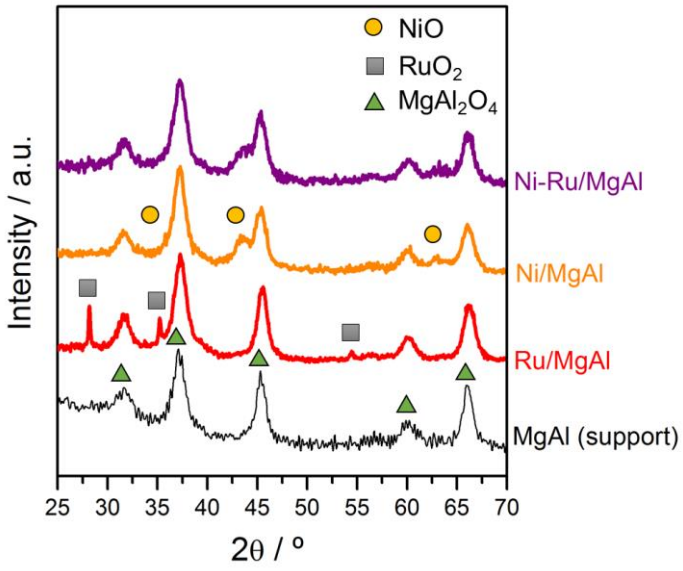

Figure 1. X-ray diffraction patterns of catalysts and support

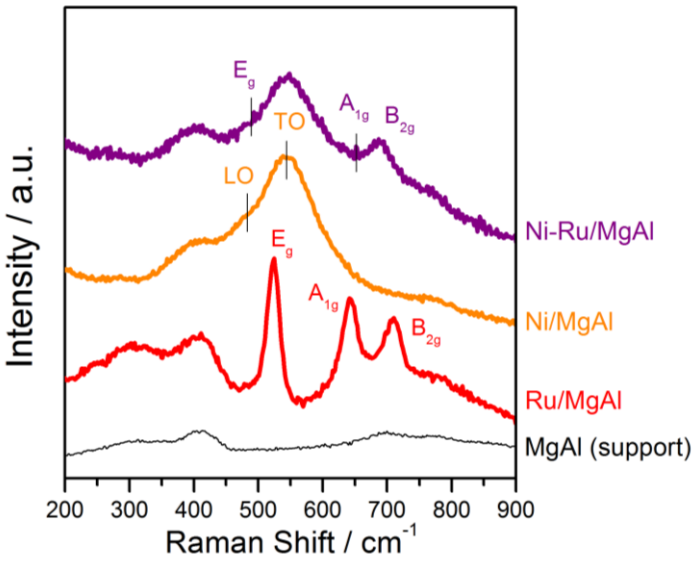

Figure 2. Raman spectra of the fresh catalysts and support

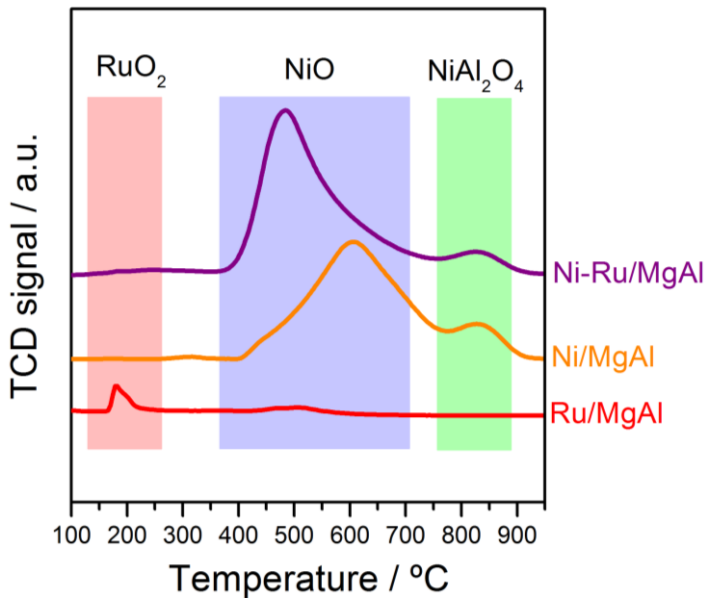

Figure 3. H_2-temperature programmed reduction (TPR) profiles of Ni-Ru/MgAl, Ni/MgAl and Ru/MgAl catalysts

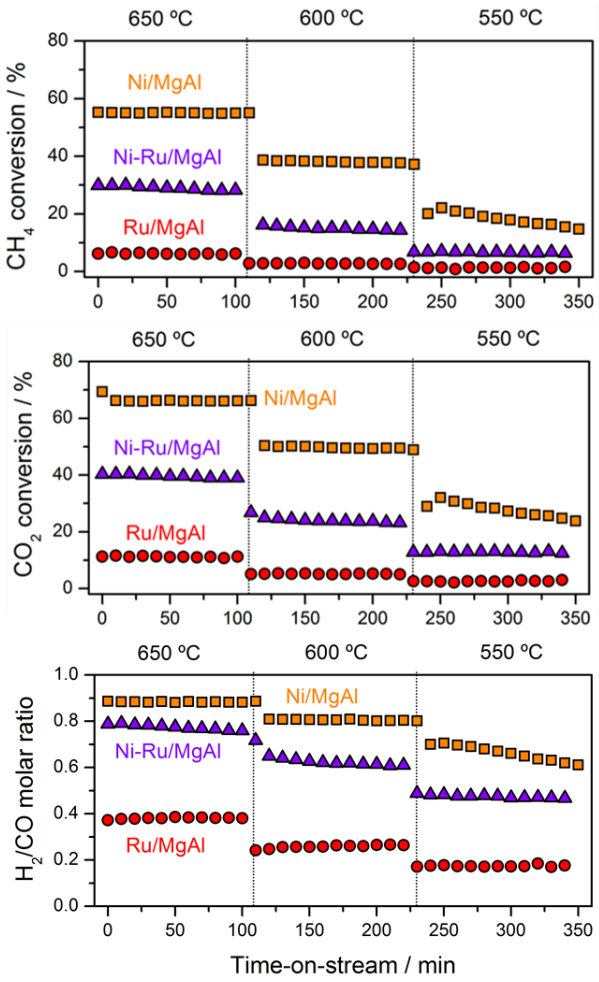

Figure 4. Catalytic performance for methane and CO_2 conversion together with the corresponding H_2/CO molar ratio as a function of time-on stream and the temperature for the three catalysts. Reaction conditions: GHSV = 150 L g^{-1} h^{-1}, atmospheric pressure, and CH_4/CO_2 = 1

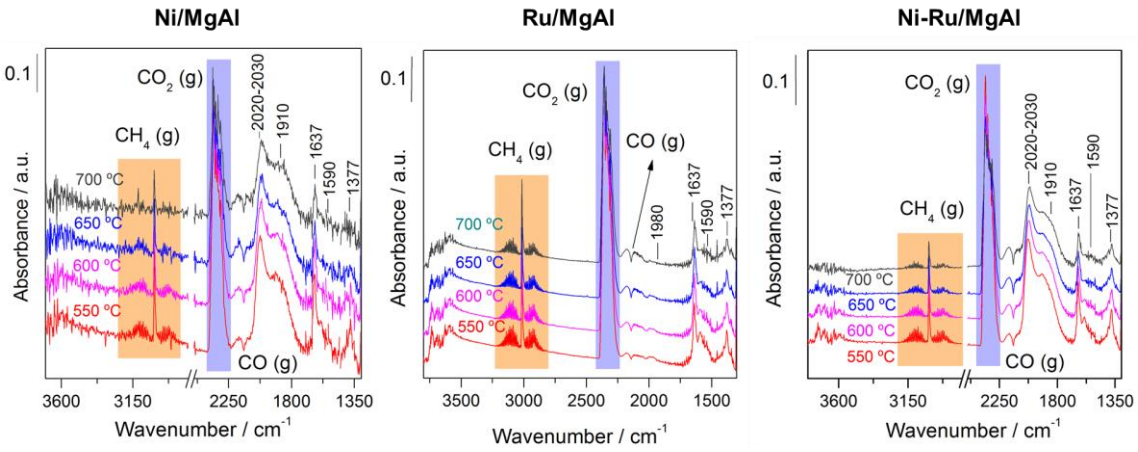

Figure 5. DRIFT spectra obtained during DRM reaction in the temperature range of 550 to 700 ºC on the three catalysts. Reaction conditions: total flow rate of 50 mL min^{-1} and $CH_4/CO_2 = 1$

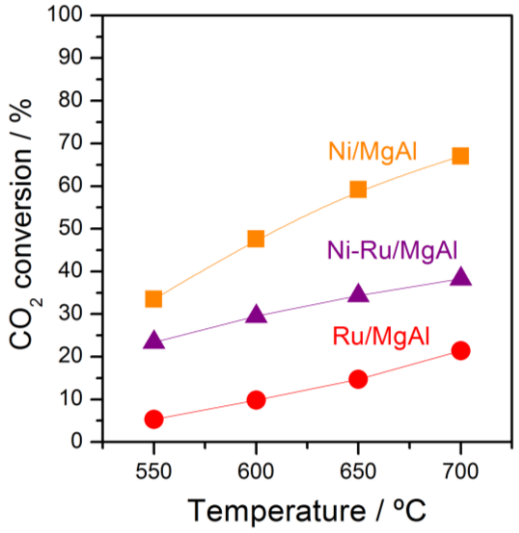

Figure 6. CO_2 conversion against the temperature measured in the DRIFTS cell under reaction conditions (total flow rate of 50 mL min^{-1} and CH_4/CO_2 = 1)

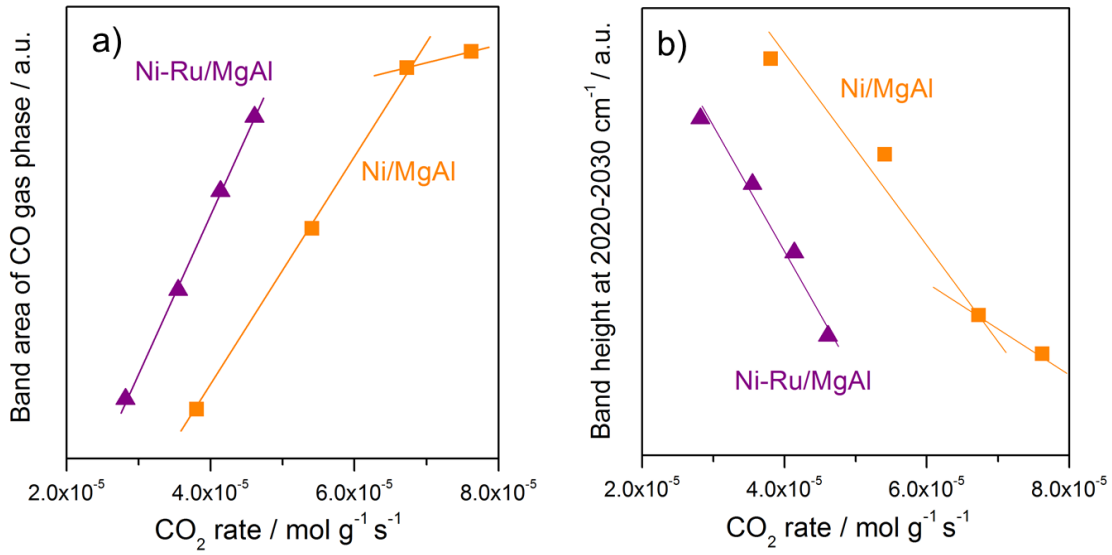

Figure 7. Correlation of band area of CO gas (left) and the band height associated to metallic carbonyl species as function of the CO_2 rate consumption on Ni/MgAl and Ni-Ru/MgAl catalysts . Reaction conditions: total flow rate of 50 mL min^{-1} and CH_4/CO_2 = 1

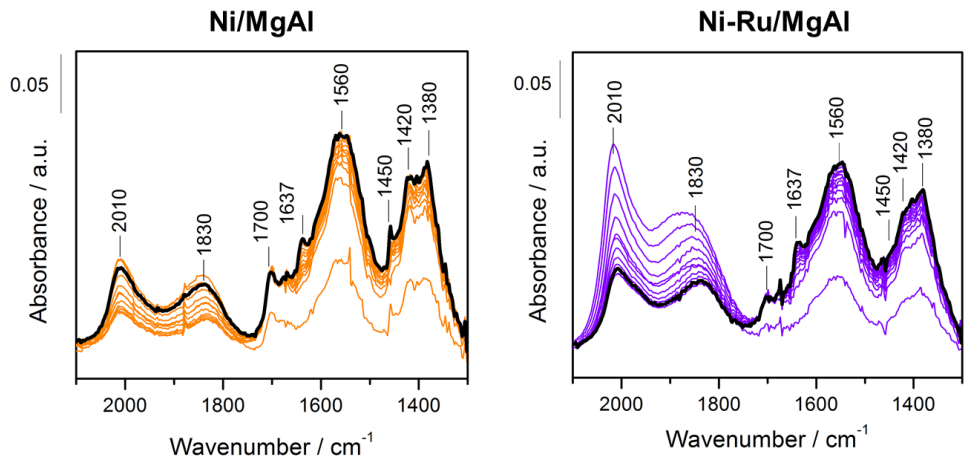

Figure 8. Evolution of DRIFTS spectra with the time on Ni/MgAl and Ni-Ru/MgAl catalysts during the adsorption of CO_2 at 550 ºC (10 vol.% CO_2 in Ar, 50 mL min^{-1}). The black line represents the last spectra obtained in each case

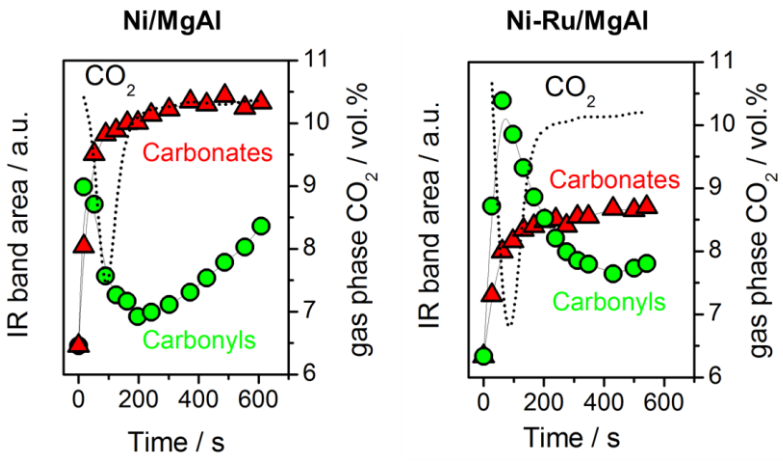

Figure 9. Evolution of the total area IR band associated to metallic carbonyls and carbonate species together with the CO_2 gas concentration profile as a function of time during the adsorption of CO_2 at 550 ºC (10 vol.% CO_2 in Ar, 50 mL min^{-1}) on Ni/MgAl and Ni-Ru/MgAl catalysts